Lipids in Health and Disease

https://doi.org/10.1186/s12944-026-02985-4

Article in Press

Investigating the role of neuroglobin in cholesterol metabolism: a spotlight on brain-derived cells

Received: 6 March 2026

Accepted: 26 May 2026

Published online: 04 June 2026

Cite this article as: Caputo S., Parente M., Colardo M. *et al.* Investigating the role of neuroglobin in cholesterol metabolism: a spotlight on brain-derived cells. *Lipids Health Dis* (2026). https://doi.org/10.1186/s12944-026-02985-4

Sara Caputo, Martina Parente, Mayra Colardo, Marco Fiocchetti, Maria Marino, Marco Segatto & Valentina Pallottini

Investigating the Role of Neuroglobin in Cholesterol Metabolism: A Spotlight on Brain-Derived Cells

Sara Caputo[1], Martina Parente[1], Mayra Colardo[2], Marco Fiocchetti[1,3], Maria Marino[1,3], Marco Segatto[2], Valentina Pallottini[1, 3,*]

[1]Department of Science, University Roma Tre, Viale Marconi 446, 00146, Rome, Italy.

[2]Department of Bioscience, University of Molise, Contrada Fonte Lappone, 86090 Pesche (IS), Italy

[3] Neuroendocrinology Metabolism and Neuropharmacology Unit, IRCSS Fondazione Santa Lucia, Via del Fosso Fiorano 64, 00143 Rome, Italy

[*] Corresponding author: Valentina Pallottini, Department of Science, University Roma Tre, Viale Marconi 446, 00146, Rome, Italy. valentina.pallottini@uniroma3.it

Abstract

Background: Cholesterol is a crucial determinant of membrane structure, signaling, and synaptic function in the central nervous system, where its homeostasis is tightly controlled to support neuronal viability and plasticity to prevent neurodegeneration. Altered brain cholesterol metabolism is increasingly recognized as a shared feature of several neurological disorders as well as age-associated cognitive decline. In parallel, neuroglobin has emerged as an endogenous neuroprotective protein in the brain, where its overexpression limits oxidative damage, mitochondrial dysfunction, and cell death in experimental models of hypoxia, ischemia, and proteinopathy. Despite extensive research on cholesterol turnover in the brain and on neuroglobin-mediated cytoprotection, the functional relationship between these two processes remains largely unexplored. The purpose of this study was to investigate whether neuroglobin modulates the cholesterol regulatory network in brain-derived cells and whether it affects the astrocyte-dependent cholesterol supply to neurons.

Methods: Human neuronal-like (SH-SY5Y) and astrocyte-like (U373) cell lines overexpressing neuroglobin were used to examine the effects of globin on key regulators of cholesterol synthesis, uptake, intracellular trafficking, and storage, as well as on susceptibility to oxidative stress. Western blot and immunofluorescence analyses were performed.

Results: The results demonstrate that neuroglobin is seemingly associated with changes in cholesterol homeostasis in a cell type-specific manner, modulating the expression of different proteins involved in cholesterol metabolism and promoting cellular cholesterol accumulation without affecting the cross-talk between astrocytes and neurons.

Conclusions: Overall, these findings suggest that NGB can be a novel modulator of cholesterol homeostasis in brain-derived cells, extending its role beyond the mitigation of oxidative stress in neurons to include defense against metabolic dysregulation.

Keywords: Cholesterol, Neuroglobin, Neuron-like cells, Astroglia-like cells, Metabolism, Rotenone.

Introduction

Cholesterol is a ubiquitous and essential cellular component that plays a critical role in maintaining membrane structure, fluidity, and the functionality of membrane-resident proteins. While virtually all cells can produce cholesterol, the liver and brain are the primary organs responsible for its synthesis in mammals. Once synthesized, cholesterol is transported to other cell types and tissues in the form of lipoprotein particles [1].

During embryonic development, the formation of the blood–brain barrier involves strict separation between the central nervous system (CNS) and the peripheral circulatory system. Consequently, lipoproteins cannot cross this barrier; thus, cholesterol metabolism in the CNS is separate from that in the rest of the body under normal physiological conditions [2]. Despite this separation, it is believed that similar mechanisms regulate cholesterol homeostasis in both the CNS and peripheral systems [3].

The regulation of cholesterol has been the focus of extensive research, primarily because its dysregulation is implicated in a wide range of diseases [4]. Indeed, since the early 20th century, cholesterol dysmetabolism has been associated with cardiovascular diseases [5] and cancer [6] and, more recently, with numerous neurological disorders [7, 8, 9]. Specifically, hereditary diseases involving mutations in cholesterol-related genes can lead to impaired brain function during infancy. Furthermore, disturbances in brain cholesterol metabolism are associated with cognitive decline during aging and in individuals with neurodegenerative disorders such as Alzheimer's disease (AD) [10], Huntington's disease (HD) [11], and Parkinson's disease (PD) [12]. Under these conditions, abnormalities in brain cholesterol levels may arise as a secondary effect of disease-related factors, exacerbating functional impairments by disrupting synaptic activity [3]. As a result, the proteins responsible for maintaining cholesterol homeostasis have garnered significant attention, particularly as potential therapeutic targets.

In this context, the discovery of neuroglobin (NGB) introduces a new challenge in the study of CNS diseases. NGB is an inducible neuroprotective globin that mitigates several hallmarks of CNS

diseases (CNDs), including impaired mitochondrial functionality, apoptosis, and oxidative stress [13, 14]. The induction of NGB overexpression has potential protective effects against neurodegeneration but also in other diseases. In fact, it appears to be modulated and to exert neuroprotective effects in Alzheimer's [15], Parkinson's, and Huntington's diseases [16] while also offering protection against ischemic heart disease [17]. Interestingly, previous studies exploring endogenous (e.g., hormones) and exogenous (e.g., plant-derived polyphenols) increases in NGB levels [18] have confirmed the protective role of NGB in neurons, revealing that neurons release NGB into the extracellular microenvironment, where it functions as an autocrine/paracrine factor, promoting cellular resistance against oxidative stress [14].

Currently, no data are available on the potential relationship between NGB and cholesterol metabolism. To date, only one study has reported that SREBP2 (sterol regulatory element binding protein-2), a transcription factor that regulates genes involved in cholesterol metabolism, is modulated in neuroglobin-knockout breast cancer cells [19]. The objective of this study was to investigate whether high levels of NGB could modulate the cholesterol regulatory network in brain-derived cells, a human neuroblastoma-derived cell line and an astrocyte-like cell line. Additionally, this study aimed to assess whether NGB affects the physiological crosstalk between astrocytes and neurons. To this end, SH-SY5Y and U373 cell lines with or without overexpression of neuroglobin were used.

2. **Materials and methods**

2.1 *Cell line, culture conditions, and treatments*

SH-SY5Y human neuroblastoma-derived cells (American Type Culture Collection, LGC Standards S.r.l., Milan, Italy) and human astrocyte-derived U373 cells were grown at 37 °C in a humidified atmosphere of 5% CO_2 supplemented with Dulbecco's modified Eagle's medium (DMEM), high glucose supplemented with L-glutamine (2 mM), non essential amino acids (1%), HEPES solution (1%), sodium pyruvate (1%), Pen-Strep solution (100 U/mL penicillin and 100 µg/mL streptomycin), and 10% fetal bovine serum (FBS) (Merck, Darmstadt, Germany). Cell lines were

authenticated periodically by amplification of multiple short tandem repeat (STR) loci, which was performed by BMR Genomics S.r.l. (Padova, Italy). SH-SY5Y and U373 cells stably overexpressing NGB containing the HA-tag sequence were obtained at the University of Roma Tre [14]. SH-SY5Y and U373 cells were grown to approximately 70% confluence and then transfected with the pCMV3-NGB-HA plasmid (Sino Biological, Beijing, China) using Lipofectamine reagent (Invitrogen, Carlsbad, CA, USA) according to the manufacturer's instructions. After selection with hygromycin-B (600 μg/mL), the cells were tested for NGB-HA expression. SH-SY5Y NGB-HA was used as a bulk population. After antibiotic selection, single U373 clones were isolated and screened for their ability to express the human NGB fused to the HA tag. SH-[MF1.1]SY5Y (SH-SY5Y Ctr-HA) and U373 (U373 Ctrl-HA) cells transfected with the empty construct were used as controls. All cells were maintained in culture under the same conditions, with hygromycin-B (300 μg/mL) used as a selective agent for stably transfected cells. The drug (2-hydroxypropyl)-β-cyclodextrin (Sigma–Aldrich/Merck, Milan, Italy) was added to SH-SY5Y cultures at the indicated concentrations (50 μM in DMEM for 24 h) after dilution from the respective stock solutions (50 mM in cell medium). Control cultures run in parallel were grown in medium culture for the indicated times.

Conditioned media were prepared according to a previously reported protocol [20]. 1×10^6 Ctrl (WT), Ctrl-HA, and NGB-overexpressing U373 cells were seeded in 10-cm culture dishes and maintained in DMEM supplemented with 10% FBS and hygromycin-B (300 μg/mL) for 24 h. The cells were subsequently washed three times with PBS (Merck Life Science, Milan, Italy) and incubated for 24 h in serum-free DMEM without hygromycin-B. The media were collected, centrifuged to remove cell debris, and immediately used to treat SH-SY5Y cells. SH-SY5Y cells were previously differentiated for 72 h in DMEM supplemented with 1% FBS and 10 μM retinoic acid (R2625; Merck Life Science, Milan, Italy). Differentiated SH-SY5Y cells were then cultured for 48 h in conditioned media from Ctrl- or NGB-overexpressing U373 cells diluted 1:1 with fresh

DMEM, with a final concentration of 1% FBS and 10 μM retinoic acid, in the presence or absence of 0.1 μM rotenone (557368, Merck Life Science, Milan, Italy) to induce a PD-like phenotype.

2.2 *Protein extraction and western blot analysis*

Cells were directly seeded in 6-well plates at 250,000 cells/well and placed at 37 °C and 95% humidity with 5% CO_2. After 3 days, the cells were then lysed by the addition of a variable amount of lysis buffer YY (50 nM HEPES (pH 7.5), 10% glycerol, 150 nM NaCl, 1% Triton X-100, 1 mM EDTA, 1 mM EGTA) supplemented with 1:1,000 protease inhibitor cocktail and 1:400 phosphatase inhibitor cocktail (Merck Life Science, Milan, Italy), depending on the experimental conditions. Cells were scraped on ice and collected in 1.5 ml tubes (Eppendorf, Germany). After 10 minutes on ice, the tubes were centrifuged at 20,000 × g for 10 min at 4 °C to remove cell debris. The pellets that contained nuclei and undissolved material were discarded, and the protein concentration of the supernatant was determined by a Bradford assay (Bio-Rad Laboratories, Hercules, CA, USA).

For immunoblotting, 30 μg of protein was added to 4x sample buffer (20% SDS, 1 M Tris HCl (pH 6.8), 0.01% Bromophenol Blu (0.01%), 100% β-mercaptoethanol and 100% glycerol), heated at 95 °C for 5 min, and loaded on a 7–13.5% acrylamide gel by adding a molecular weight marker (Novex Sharp) on one side of the gel. The proteins were subsequently blocked on nitrocellulose membranes using a Trans-Blot Turbo Transfer System (Bio-Rad Laboratories, Milan, Italy) for 10 min at 25 V. The membranes were then blocked with fat-free milk or BSA (5% in Tris-buffered saline 0,138 M NaCl, 0,027 M KCl, 0,025 M Tris-HCl, and 0,05% Tween-20, pH 6,8) for 1 h at room temperature (RT), and then incubated at 4° C overnight with the following primary antibodies: ACC (Cell Signaling Technology, cs-3662S dilution 1:1,000), AMPK (Santa Cruz Biotechnology Technology, sc-25792, dilution 1:1,000), P-AMPK (Cell Signaling Technology, #2531 dilution 1:1,000), APOA1 (Sigma–Aldrich, SAB-5300518-100, dilution 1:1,000), APOE (Santa Cruz Biotechnology, sc-390925, dilution 1:1,000), HMCGR (Abcam Limited, ab-174830, dilution 1:1,000), P-HMCGR (Thermo Fisher Scientific, PA5-114581, dilution 1:1,000), and LDLR (Abcam Limited, ab-30532, dilution 1:1000), LRP1 (Santa Cruz biotechnology, sc-25469, dilution 1:1,000),

NGB (ProteinTech, 13499-1AP, dilution 1:1,000), NPC1 (Novus Biologicals, NB400-148, dilution 1:1,000), Squalene Synthetase (Santa Cruz biotechnology, sc2-71602, dilution 1:1000), SR-B1 (Abcam Limited, ab-52629, dilution 1:1,000), SREBP1 (Santa Cruz biotechnology, sc-366, dilution 1:1,000), SREBP2 (Abcam Limited, ab-30682, dilution 1:1,000), TMEM97 (Novus Biologicals, NBP1-30436, dilution 1:1,000), Vinculin (Sigma-Aldrich, V9131, dilution 1:40,000) and Tubulin (Sigma-Aldrich, T6074, dilution 1:40,000).

The membranes were subsequently incubated for 1 h with horseradish peroxidase-conjugated secondary IgG antibodies (Bio-Rad Laboratories, Milan, Italy). Protein-antibody immunocomplexes bound to nitrocellulose were visualized by using clarity ECL Western blotting (Bio-Rad Laboratories, Milan, Italy, #1705061), and chemiluminescence acquisition was carried out through a ChemiDoc XRS+Imaging System (Bio-Rad Laboratories Hercules, CA, USA). Densitometric analysis was performed by ImageJ. Represented values were derived from the ratio between arbitrary units obtained from the protein band and the respective protein loading control. The data are expressed as fold changes versus the control group.

2.3 *Filipin staining*

The cellular distribution of unesterified cholesterol was visualized by filipin complex staining (Merck Life Science, Milan, Italy), as previously described [21]. A filipin stock solution (10 mg/mL in EtOH) was freshly prepared prior to use. SH-SY5Y and U373 cells were seeded on 8-well high μ-Slide (Ibidi, Cells in focus) at 8,000 cells per well previously coated with poly-D-lysine (100 mg/mL).

To analyze the distribution of unesterified cholesterol, the cells were fixed with 4% paraformaldehyde (PFA) and rinsed 3 times with PBS. The cells were stained with 0.2 mL of Filipin working solution (50 μg/mL) for 2 hours at room temperature in the dark. After staining, the cells were washed three times to remove excess dye. Finally, the cells were viewed through a Nikon A1R confocal microscope (40× objective, 3× zoom) (Nikon Corporation, Tokyo, Japan) using a UV filter set (340–380 nm excitation). Images were acquired at 40× magnification and analyzed by

using ImageJ, after which the average intensity of fluorescence per cell was measured and normalized to the number of nuclei.

2.4 Cholesterol quantification assays

Total cholesterol levels were quantified using a commercially available colorimetric assay kit (Cholesterol Quantitation Kit-MAK043; Sigma–Aldrich, Germany; Catalog Number CS0005). The detection range of the assay was 1–5 μg/dL. The procedure provided in the manufacturer's manual was followed for the total cholesterol assay, and the results are expressed as the cholesterol concentration in ng/1,0 × 10^6 cells. Briefly, the assay detects total cholesterol (cholesterol and cholesteryl esters) when cholesterol esterase is included in the reaction. The enzymatic assay results in a colorimetric product proportional to the cholesterol present in the sample.

2.5 Oil Red O staining

Neutral lipids, including triglycerides, cholesterol esters and free cholesterol, were visualized by using Oil Red O staining (Sigma–Aldrich). SHSY5Y cells were seeded on a μ-Slide 8-Well High (Ibidi, Cells in focus) at 8,000 cells per well previously coated with poly-D-lysine (100 mg/mL). After 3 days, the cells were fixed in 4% paraformaldehyde (PFA) and rinsed 3 times with PBS. The fixed cells were incubated with 60% isopropanol for 5 min and then washed with distilled water. The cells were subsequently stained with 0.5 mL of Oil Red O working solution (6:1 distilled water, filtered) for 15 min at room temperature, after which the plate was kept on a horizontal shaker. Afterward, the cells were washed 3 times with distilled water to eliminate the excess stain. The nuclei were revealed by DAPI staining (Merck Life Science, Milan, Italy) in PBS (1:2,000, 5 min). Oil Red O autofluorescence was viewed through a Nikon A1R confocal microscope (40× objective, 3× zoom) (Nikon Corporation, Tokyo, Japan) using a UV filter set (340–380 nm excitation). Images were acquired at 40× magnification and analyzed by using ImageJ, after which the average intensity of fluorescence per cell was measured and normalized to the number of nuclei.

2.6 Immunofluorescence

2.6.1 *Immunofluorescence in SH-SY5Y cells*

SH-SY5Y cells were cultured on 8-well high µ-Slide (Ibidi, Cells in focus, #80827) at 8,000 cells per well and treated as indicated. Following treatment, the cells were washed three times with phosphate-buffered saline (PBS), chemically fixed with 4% paraformaldehyde (PFA) for 10 min, and rinsed 3 times with filtered PBS. The cells were permeabilized (0.05% Triton X-100 in PBS) for 10 min, incubated for 45 min with blocking solution (3% filtered bovine serum albumin in PBS) and then incubated overnight at 4 °C with primary antibodies (1% bovine serum albumin in PBS) against SREBP2 (Santa Cruz, sc-13552, dilution 1:40) and LAMP2 (Santa Cruz, sc-18822, dilution 1:1,000). After being incubated, the cells were washed and reacted for 1 h at room temperature with the appropriate secondary antibodies (Thermo Fisher Scientific, #A-10040; goat anti-rabbit secondary antibody conjugated to Alexa Fluor 546; dilution 1:1,000; or #A-11001; goat anti-mouse secondary antibody conjugated to Alexa Fluor 488; dilution 1:500). The fluorescence was visualized and digitized using a Nikon A1R confocal microscope (40× objective, 3× zoom) (Nikon Corporation, Tokyo, Japan) with a UV filter set (340–380 nm excitation). Images were acquired at 40× magnification and analyzed by using ImageJ software (Version 8; National Institutes of Health, Bethesda, MD, USA), after which the average intensity of fluorescence per cell was measured and normalized to the number of nuclei.

2.6.2 *Immunofluorescence in U373*

U373 cells were seeded onto sterilized coverslips coated with poly-L-lysine (P6282; Merck Life Science, Milan, Italy) at a density of 120,000 cells per well. The cells were fixed for 10 min at room temperature in 4% paraformaldehyde (D1408; Merck Life Science, Milan, Italy) in PBS (pH 7.4). The cells were then permeabilized for 5 min with 0.1% Triton X-100 (Merck Life Science, Milan, Italy) in PBS. Nonspecific binding was blocked for 1 h at room temperature with 3% bovine serum albumin (BSA; A3912; Merck Life Science, Milan, Italy) in PBS containing 0.1% Triton. The cells were subsequently incubated overnight with the following primary antibodies: anti-NGB (ProteinTech, 13499-1AP, dilution 1:100) and anti-SREBP2 (Santa Cruz Biotechnology, sc-13552, dilution 1:50). The cells were subsequently incubated for 1 h with an Alexa Fluor 488-conjugated

goat anti-rabbit secondary antibody (Thermo Fisher Scientific, Waltham, MA, USA; A27034) and an Alexa Fluor 555-conjugated goat anti-mouse secondary antibody (Thermo Fisher Scientific, Waltham, MA, USA; A28180). Nuclei were visualized by DAPI staining, and coverslips were subsequently mounted using Fluoroshield mounting medium (F6182; Merck Life Science, Milan, Italy). The samples were examined with a confocal microscope (TCS SP8; Leica, Wetzlar, Germany) at 40× magnification, and images were acquired with LAS X software (version 3.5.5; Leica Camera, Wetzlar, Germany) on Windows 10. Protein expression levels were quantified as the mean fluorescence intensity normalized to the cell area using ImageJ software (v.154d; National Institutes of Health, Bethesda, MD, USA) on Windows 11.

2.7 Quantitative evaluation of neuronal morphology

Neuronal morphology in SH-SY5Y cells was assessed by acquiring images using an inverted microscope (Eclipse 7 s100; Nikon Corporation, Tokyo, Japan), and morphometric analysis was performed using ImageJ software for Windows (v.154d; National Institutes of Health, Bethesda, MD, USA). The total number of cells (expressed as a percentage relative to the control) and the average neurite length (expressed as a percentage of the control) were evaluated. Morphological assessments were carried out in multiple experiments in which at least three images were analyzed.

2.8 Statistical analysis

Statistical analysis was performed using a two-tailed unpaired Student's t test for relative values and one-way analysis of variance (ANOVA), followed by Tukey's post hoc test. The asterisks indicate statistically significant differences based on p values (*=p< 0,05; **=p<0,01; ***=p<0,001). The data are displayed as the mean ± standard deviation (SD). Statistical analysis and graphical illustrations were performed with GraphPad Prism v8.0 (*GraphPad Software*, Inc., San Diego, CA, USA) for Windows.

3. Results

To perform this study, human neuroblastoma cells (SH-SY5Y) were used to generate two cell models: one transfected with the NGB-HA plasmid for overexpressing NGB (NGB-HA) and a control group transfected with the empty construct (Ctrl-HA). As shown in Figure 1A, NGB protein expression was strongly increased in NGB-HA-treated cells compared with control cells, confirming the effectiveness of NGB overexpression in the experimental model. To study the impact of NGB on cholesterol metabolism, the expression of SREBP2, a transcription factor that regulates genes involved in cholesterol metabolism [22], was first evaluated in overexpressing and control cells. Both the total form (Figure 1B panel 1) and its active nuclear form (nSREBP2) (Figure 1B panel 2) were increased in NGB-HA cells compared with those in control cells, a finding further confirmed by immunofluorescence (Figure 1C panels 1 and 2).

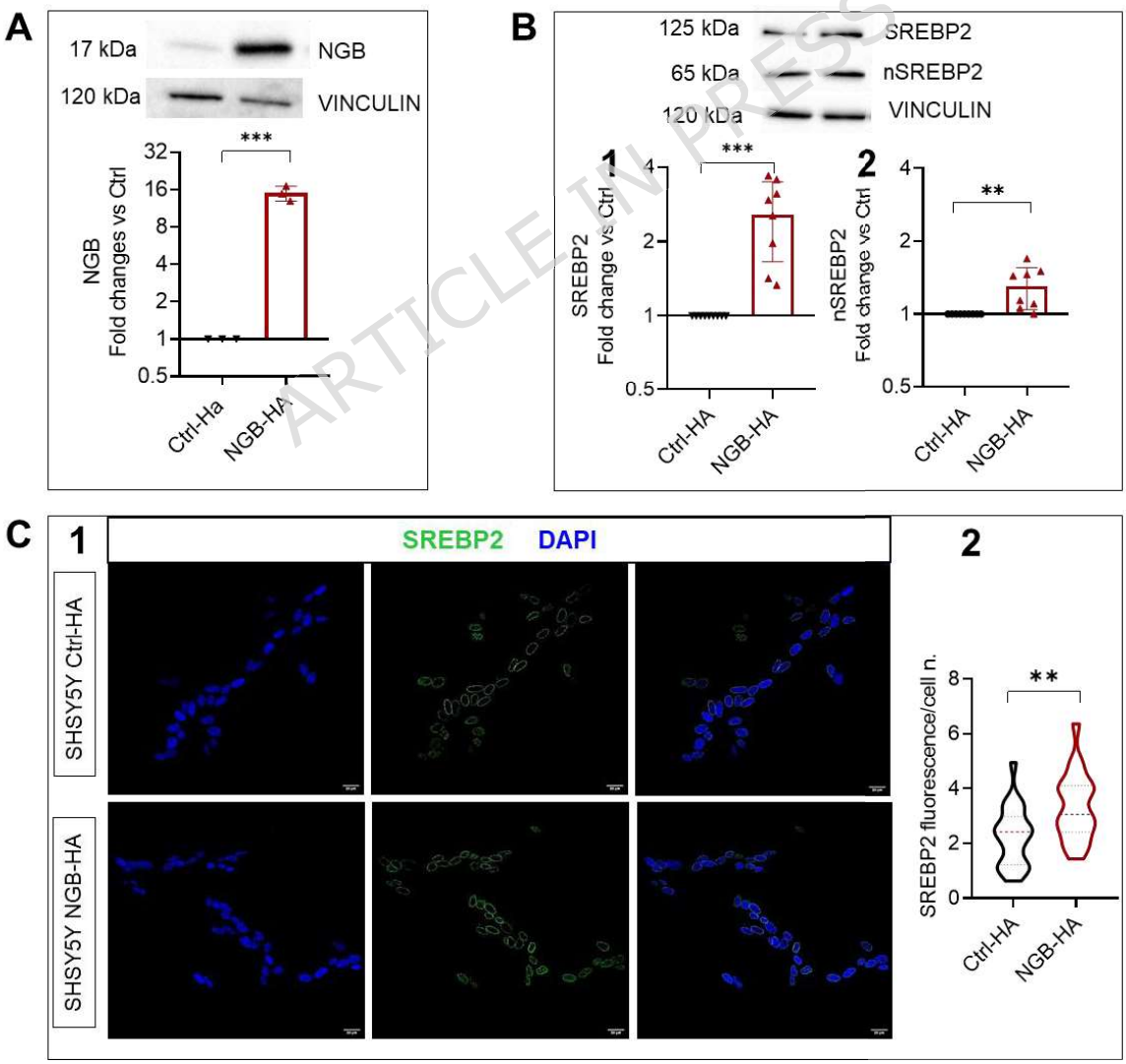

Figure 1. Effects of neuroglobin on transcriptional regulators of cholesterol homeostasis. (Panel A) On the top, a representative Western blot is shown; on the bottom, the densitometric analyses of the bands of Neuroglobin (NGB) protein levels in SH-SY5Y Ctrl-HA and NGB-HA SH-SY5Y cells are shown. VINCULIN was used as a loading control (n=3 biological replicates, each analyzed in technical triplicate). (Panel B) On the top, a representative Western blot; on the bottom, densitometric analyses of the protein expression levels of full-length SREBP2 (1) and its cleaved nuclear form (nSREBP2) (2) in Ctrl-HA and NGB-HA SH-SY5Y cells are shown. VINCULIN was used as a loading control. (n=3 biological replicates, each analyzed in technical triplicate). The numbers above the horizontal bars represent the mean values relative to the baseline (Ctrl-HA). (Panel C1) Representative fluorescence micrographs (40x objective, 3x zoom; scale bar, 20 μm) of SREBP2 (green) and nuclear DAPI staining (blue) in SH-SY5Y Ctrl-HA and NGB-HA cells. (Panel C2) Quantification of SREBP2 fluorescence intensity per cell normalized to the number of nuclei. (n= 4 biological replicates, with 10 randomly selected fields analyzed per experimental group). The data are presented as the means ± SDs. Statistical analysis was performed using an unpaired Student's t test (**$p < 0.01$, ***$p < 0.001$).

The observed increase in nSREBP2 is corroborated by a concomitant increase in 3-hydroxy 3-methylglutheryl coenzyme A reductase (HMGCR) (Fig 2A panel 1), the rate-limiting enzyme of the mevalonate (MVA) pathway, which is responsible for cholesterol biosynthesis. A similar trend is observed for the phosphorylated (inactive) form of HMGCR (P-HMGCR) (Figure 2A panel 2). Consequently, the ratio of total to phosphorylated HMGCR (Figure 2A panel 3) is reduced in NGB-HA cells, indicating a lower proportion of the enzyme in its active state in cells overexpressing NGB. Consistent with these observations, the phosphorylation state of AMP-activated protein kinase (AMPK), reflecting its activation, was increased in NGB-HA cells (Figure 2B). AMPK is responsible for phosphorylating HMGCR, thereby inhibiting its enzymatic activity [23]. Collectively, these results indicate that despite the upregulation of HMGCR protein expression, its

enzymatic activity is diminished in NGB-overexpressing cells, possibly due to increased AMPK-mediated phosphorylation, suggesting a potential reduction in cholesterol synthesis. To further validate this hypothesis, the levels of squalene synthase (SQS), another key enzyme in the mevalonate MVA pathway involved in cholesterol biosynthesis, were measured. SQS levels were significantly lower in NGB-overexpressing cells than in control cells (Figure 2C), thereby supporting the proposed hypothesis. Therefore, its primary transcription factor, sterol regulatory element binding protein 1 (SREBP-1), was analyzed [24], and a significant reduction in both its full-length form and its transcriptionally active nuclear form (nSREBP-1) was observed (Figure 2D panels 1 and 2). To further support these findings, the levels of acetyl-CoA carboxylase (ACC), a well-known SREBP-1 target enzyme, were also decreased (Figure 2E). Since ACC is the key enzyme in fatty acid synthesis, the neutral lipid content decreased in NGB-HA cells (Figure 2F panels 1 and 2).

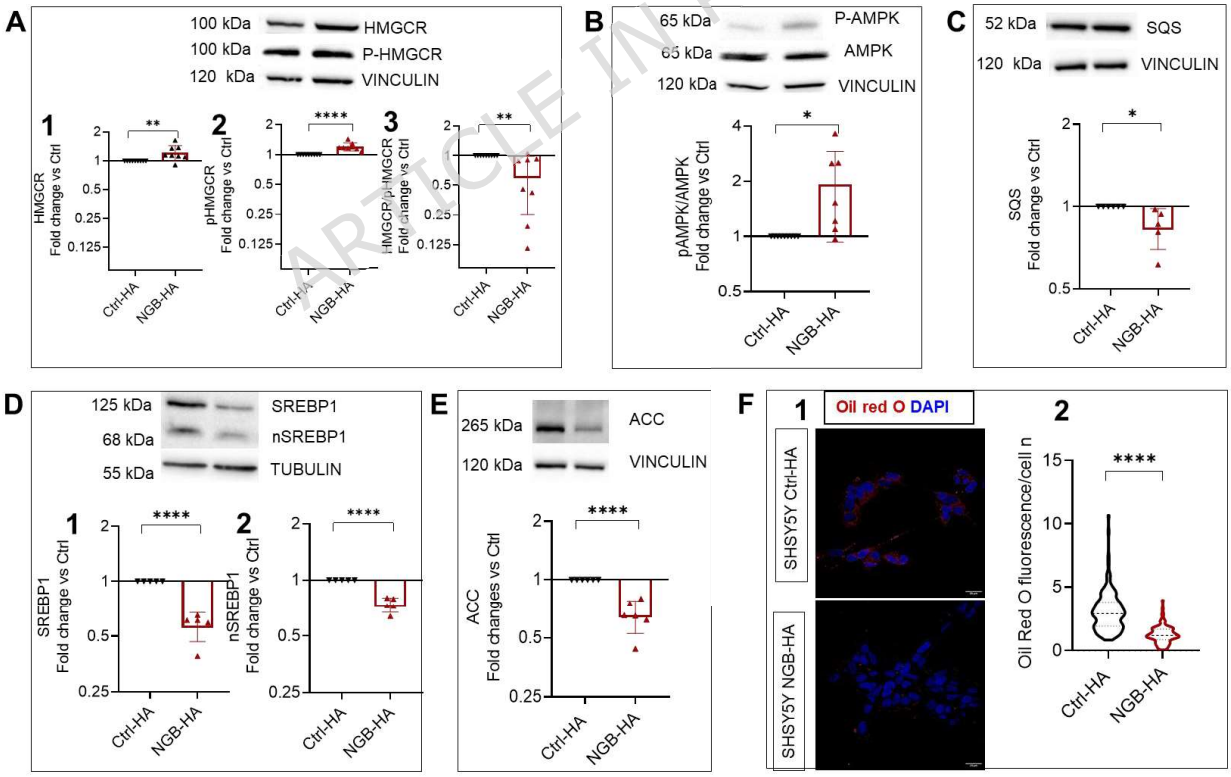

Figure 2. Effects of NGB on enzymes that mediate cholesterol and fatty acid synthesis. (Panels A-E) Representative Western blots and densitometric analysis of HMGCR (A1), phosphorylated

HMGCR (pHMGCR) (A2), the HMGCR/pHMGCR ratio (A3), pAMPK/AMPK (B), squalene synthase (SQS) (C), full-length SREBP1 (D1), the cleaved nuclear form (nSREBP1) (D2), and acetyl-CoA carboxylase (ACC) (E) in SH-SY5Y Ctrl-HA and NGB-HA cells. The numbers above and below the horizontal bars represent the mean values relative to the baseline (Ctrl-HA). VINCULIN or TUBULIN was used as a loading control. (*n*=3 biological replicates, each analyzed in technical triplicate). (Panel F1) Representative fluorescence micrographs (40×; scale bar, 20 μm) of neutral lipid droplets stained with Oil Red O (red) and nuclei stained with DAPI (blue) in SH-SY5Y Ctrl-HA and NGB-HA cells. (Panel F2) Quantification of Oil Red O fluorescence intensity per cell normalized to the number of nuclei. (*n*=4 biological replicates, with 10 randomly selected fields analyzed per experimental group). The data are presented as the means ± SDs. Statistical analysis was performed using an unpaired Student's t test (* p<0.01, **p < 0.01, ****p<0.0001).

The reduction in MVA pathway activity could suggest a negative modulation of the intracellular cholesterol content; however, analysis of free cholesterol by filipin staining (Figure 3A panels 1 and 2) and measurement of total cholesterol levels (Figure 3B) revealed the opposite results. In fact, an increase in the intracellular cholesterol content in NGB-HA-treated cells was observed. Thus, key proteins involved in cholesterol uptake were studied, and the results revealed significant increases in both low-density lipoprotein receptor (LDLR) and LDL receptor-related protein 1 (LRP1) expression in NGB-overexpressing cells (Figure 3C and 3D). Conversely, a decrease in scavenger receptor class B type 1 (SR-B1) (Figure 3E), which mediates HDL transport, was observed [25]. To confirm the modulation of the aforementioned receptors, the intracellular levels of APOE and APOA1, the apolipoproteins associated with LDL and HDL, respectively, were measured. This analysis revealed increased APOE levels (Figure 3F) and reduced APOA1 levels (Figure 3G).

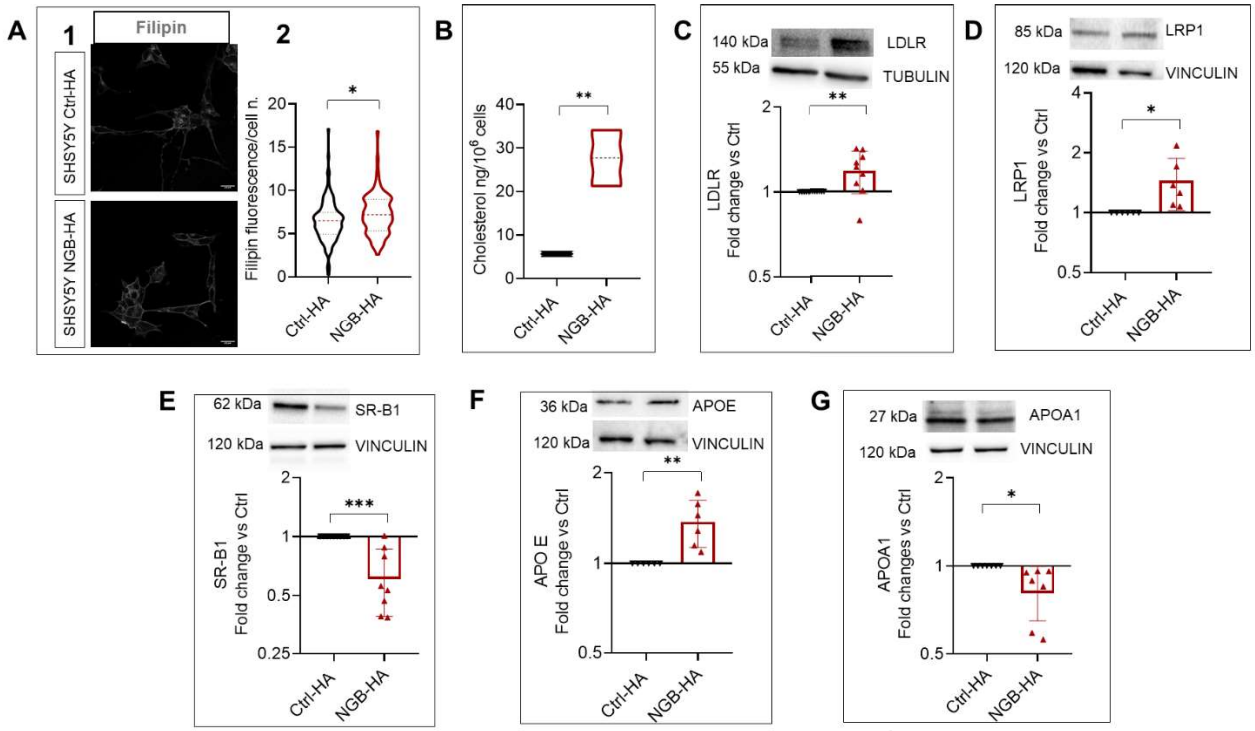

Figure 3. Neuroglobin overexpression alters cholesterol content and lipoprotein receptor expression in SH-SY5Y cells. (Panel A) Representative images (1) and quantitative analysis (2) of filipin staining in SH-SY5Y Ctrl-HA and NGB-HA cells normalized to the number of nuclei. (*n* =3 biological replicates, with 10 randomly selected fields analyzed per experimental group). (Panel B) Total cholesterol content per 10^6 cells measured by an enzymatic assay in SH-SY5Y Ctrl-HA and NGB-HA cells. (Panels C–G) Representative Western blots on the top and densitometric analysis of LDLR (C), LRP1 (D), SRB1 (E), APOE (F), and APOA1 (G) expression in SH-SY5Y Ctrl-HA and NGB-HA cells. The numbers above or below the horizontal bars represent the mean values relative to the baseline (Ctrl-HA). VINCULIN or TUBULIN was used as a loading control. (*n*=3 biological replicates, each analyzed in technical triplicate). The data are presented as the mean±SD of independent experiments. Statistical analysis was performed using an unpaired Student's t test (*p<0.05, **p<0.01, ***p<0.001).

Under physiological conditions, cholesterol accumulation is expected to inhibit the nuclear translocation of SREBP2 through the classical negative feedback mechanism operating at the

endoplasmic reticulum (ER) [26]. However, such inhibition does not occur, as shown in Figure 1. Therefore, it has been hypothesized that cholesterol is internalized but remains sequestered within the endosome–lysosome system. To investigate this, immunofluorescence analysis of lysosomal-associated membrane protein 2 (LAMP2), a typical lysosomal marker, was performed. Increased LAMP2 expression was observed, suggesting possible expansion of these intracellular organelles (Figure 4A panels 1 and 2). To further investigate this hypothesis, the levels of Niemann–Pick type C1 (NPC1), a protein responsible for transporting cholesterol out of lysosomes and redistributing it to the plasma membrane and other cellular organelles, were analyzed [27]. The results revealed a decrease in NPC1 protein content (Figure 4B), suggesting that lysosomal cholesterol accumulation is possibly due to impaired cholesterol efflux from lysosomes. These results are consistent with the reduced levels of SREBP1 observed, as it is the primary transcription factor that regulates NPC1 expression [28]. Furthermore, an increase in transmembrane protein 97 (TMEM97) protein levels (Figure 4C), which is typically regulated in opposition to NPC1, was observed [29, 4]. The increase in TMEM97 further corroborates and supports the evidence of enhanced cholesterol uptake; in fact, together with progesterone receptor membrane component 1 (PGRMC1), the three elements that seem to configure the lipid/cholesterol receptor in the cell membrane are TMEM97 and LDLR [30, 4].

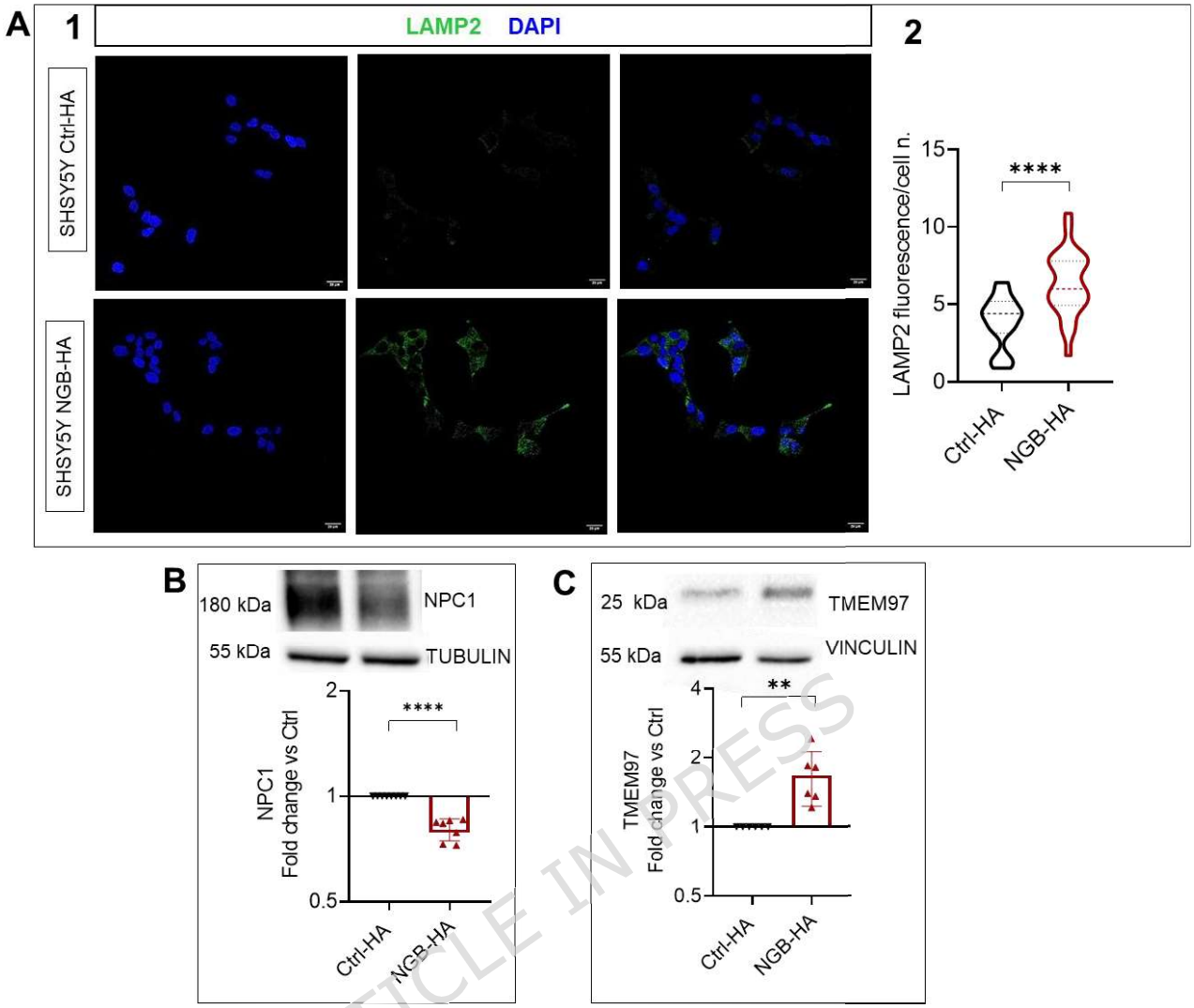

Figure 4. Effects of NGB on intracellular cholesterol distribution and transport. (Panel A1) Representative fluorescence micrographs (40×; scale bar, 20 μm) of LAMP2 (green) and nuclear DAPI staining (blue) in SH-SY5Y Ctrl-HA and NGB-HA cells. (Panel A2) Quantification of LAMP2 fluorescence intensity per cell normalized to the number of nuclei. (*n*=4 biological replicates, with 10 randomly selected fields analyzed per experimental group). (Panels B-C) Representative Western blots (top) and densitometric analysis (bottom) of NPC1 (B) and TMEM97 (C) in SH-SY5Y Ctrl-HA and NGB-HA cells. The numbers above or below the horizontal bars represent the mean values relative to the baseline (Ctrl-HA). TUBULIN and VINCULIN were used as loading controls. (*n*=3 biological replicates, each analyzed in technical triplicate). The data are

presented as the means±SDs. Statistical analysis was performed using an unpaired Student's t test (**p<0.01, ****p<0.0001).

The data obtained thus far suggest that NGB overexpression may induce a decrease in cholesterol synthesis and an increase in its uptake but that some of these lipids remain trapped within lysosomes, leading to the expansion of these organelles and possibly a reduced redistribution of cholesterol to the endoplasmic reticulum. This impaired trafficking may prevent the negative feedback regulation exerted by cholesterol [26]. To determine whether this is indeed the case, both NGB-HA and Ctrl-HA cells were treated with β-cyclodextrin (β-CD), which sequesters and redistributes cholesterol to the endoplasmic reticulum and various cellular organelles [28] , to assess whether normal SREBP2 regulation is restored. After β-CD treatment, the cholesterol content in NGB-overexpressing cells decreased (Figure 5A panels 1 and 2), and nSREBP2 levels were restored (Figure 5B panels 1 and 2).

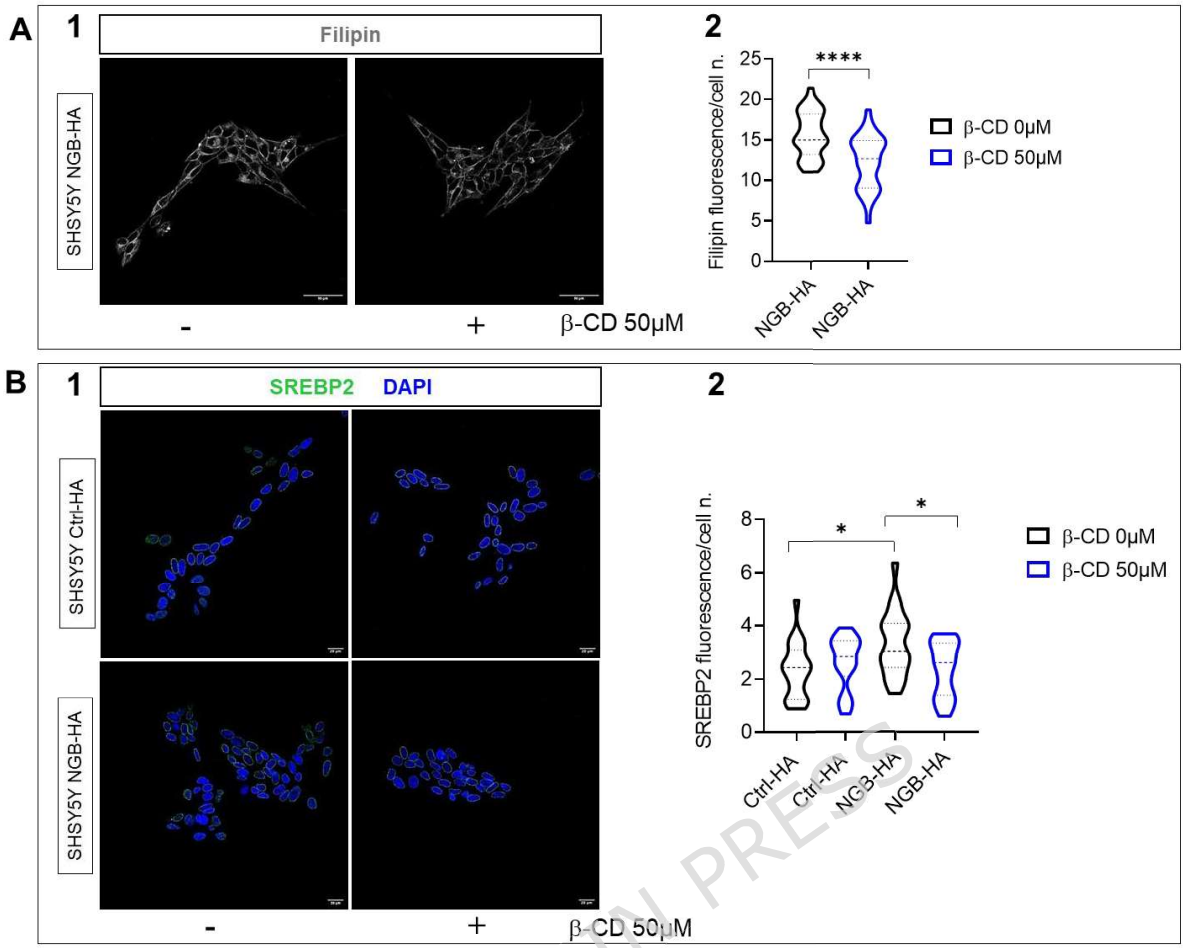

Figure 5. Effects of beta-cyclodextrin on NGB-induced cholesterol accumulation. (Panel A) Representative images (1) and quantitative analysis (2) of filipin staining in SH-SY5Y NGB-HA cells in the presence or absence of β-cyclodextrin (β-CD, 50 μM, 24 h), normalized to the number of nuclei. (*n* =4 biological replicates, with 10 randomly selected fields analyzed per experimental group). (Panel B). Representative images (1) and quantitative analysis (2) of SREBP2 fluorescence intensity per cell, normalized to the number of nuclei in SH-SY5Y Ctrl-HA and NGB-HA cells in the presence or absence of β-cyclodextrin (β-CD, 50 μM, 24 h), normalized to the number of nuclei. (*n* =4 biological replicates, with 10 randomly selected fields analyzed per experimental group). The data are presented as the mean ± SD. Statistical analysis was performed using an unpaired Student's t test (****$p<0.0001$) in Panel A and one-way ANOVA followed by Tukey's post hoc test (*$p<0.05$) in Panel B.

To assess whether the NGB-dependent cholesterol remodeling observed in neurons extends to astrocytes, the primary cholesterol supplies to neurons in mature brains [2], and the expression of proteins involved in the cholesterol homeostasis network in U373 (astrocyte-like) cells overexpressing or not overexpressing NGB (Fig. 6A panels 1 and 2) were estimated. These cells provide cholesterol to neurons in mature brains [2]. Unlike SH-SY5Y cells, these astrocyte-like cells did not exhibit an increase in SREBP2 expression (Fig. 6B panels 1 and 2). However, NGB overexpression in U373 cells induced alterations in the levels of several cholesterol metabolism proteins, including elevated HMGCR (Fig. 6C) and APOE (Fig. 6F), which is consistent with observations in SH-SY5Y cells. In U373 cells, increased levels of SQS (Fig. 6D) and NPC1 (Fig. 6G) were also noted in NGB-overexpressing cells, whereas no changes in LDLR occurred (Fig. 6E); these findings differ from those observed in SH-SY5Y cells. Nonetheless, free cholesterol accumulation was detected in U373 cells (Fig. 6H panels 1 and 2), indicating that NGB overexpression affects cholesterol metabolism in astrocyte-derived cells, albeit through partially distinct mechanisms.

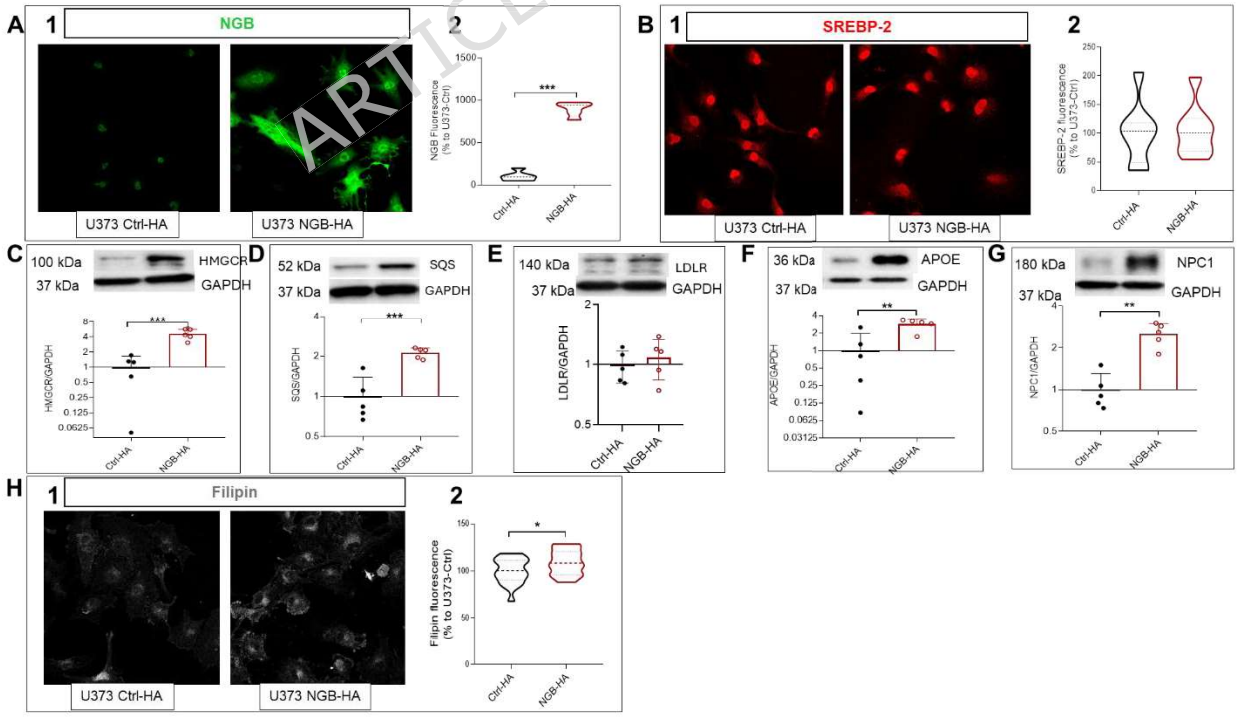

Figure 6. NGB overexpression differentially regulates key proteins involved in cholesterol metabolism and increases the free cholesterol content in U373 cells. (Panel A) Immunofluorescence (1) and respective quantitative analysis of NGB (2) in U373 Ctrl-HA and NGB-HA cells. (Panel B) Immunofluorescence (1) and respective quantitative analysis (2) of SREBP2 in U373 Ctrl-HA and NGB-HA U373 cells. (n = 6 different experiments). (Panels C–G) Representative Western blot (top) and densitometric analysis (bottom) of HMGCR (C), SQS (D), LDLR (E), APOE (F), and NPC1 (G) in U373 Ctrl-HA and NGB-HA U373 cells. The numbers above the horizontal bars represent the mean values relative to the baseline (Ctrl-HA). n=6 biological replicates. GAPDH was used as a loading control. (Panel H) Representative images (1) and corresponding quantitative analysis (2) of filipin staining performed on U373 Ctrl-HA and NGB-HA U373 cells. (n=10 different experiments). The data are presented as the means±SDs. Statistical analysis was performed by using an unpaired Student's t test. (*p<0.05, **p<0.01, ***p<0.001).

Given the observed intracellular accumulation of APOE in U373 cells, NGB overexpression may increase the release of APOE-containing lipoproteins. This astrocyte-mediated process is essential for the supply of cholesterol to neurons and for neuronal survival under insults such as rotenone [31]. To investigate this functional aspect, differentiated SH-SY5Y neuronal cells were exposed to conditioned medium (CM) from control or NGB-overexpressing U373 cells, followed by rotenone treatment (Figure 7A). The results demonstrated that both U373 Ctrl-HA CM and U373 NGB-HA CM enhanced neuronal survival following rotenone exposure, as indicated by the increased cell number (Figure 7B). Although neurite length was not affected (Figure 7C), these findings highlight the ability of astrocyte-conditioned media to promote neuronal viability, irrespective of NGB overexpression.

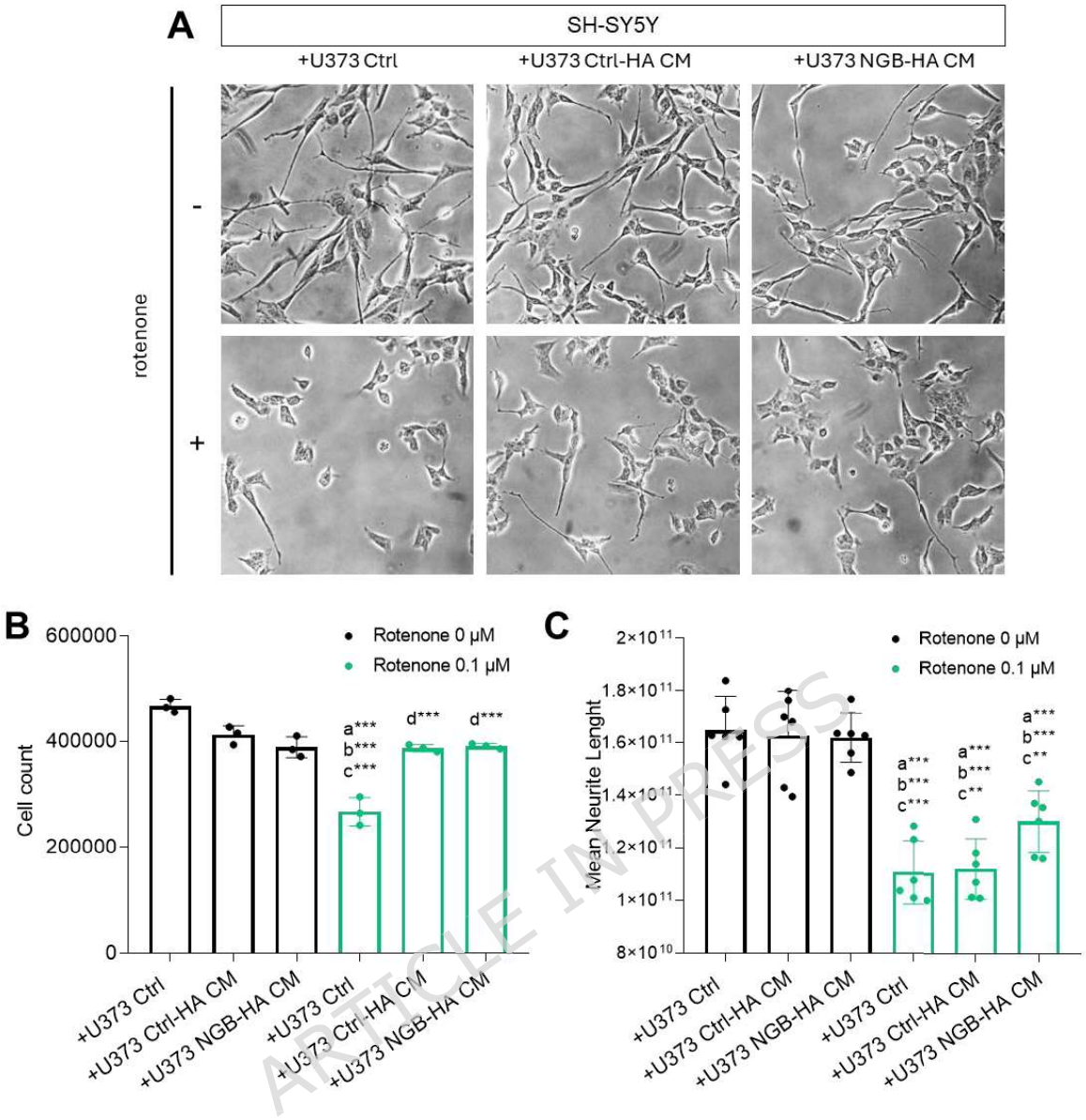

Figure 7. Conditioned medium (CM) from U373 cells enhances the survival of rotenone-treated differentiated SH-SY5Y cells without rescuing neuronal morphology. (Panel A) Representative brightfield images, (B) cell count, and (C) respective quantitative analysis of the neurite length of SH-SY5Y cells cultured either alone (Ctrl) or with CM derived from U373 astrocytes expressing Ctrl-HA or NGB-HA, with or without rotenone (0.1 µM). (*n* = 6 independent experiments). The data are presented as the means±SDs. Statistical analysis was performed using one-way ANOVA followed by Tukey's post hoc test. "a" indicates statistical significance vs. the Ctrl (vehicle), "b" indicates statistical significance vs. the U373-Ctrl-HA (vehicle) group, "c" indicates statistical

significance vs. the U373-NGB-HA (vehicle), and “d” indicates statistical significance vs. the Ctrl (rotenone) group. (**p<0.01, ***p<0.001).

4. Discussion

Cholesterol metabolism in the CNS plays a pivotal role in maintaining neuronal physiology and supporting membrane integrity, synaptogenesis, and signal transduction [3]. Unlike peripheral tissues, the central nervous system (CNS) depends on local *de novo* synthesis and tightly regulated transport across the blood–brain barrier. Disruptions in these processes are linked to impaired cellular homeostasis [32]. NGB, an inducible heme-binding protein predominantly expressed in neurons and astrocytes, has been implicated in diverse neuroprotective mechanisms, including ROS/RNS scavenging, inhibition of cytochrome c release, apoptosis blockade, and activation of pro-survival pathways such as AKT [33, 34, 35]. *In vivo* and *in vitro* evidence further indicates that NGB overexpression mitigates protein aggregation and toxicity under stress conditions such as hypoxia, ischemia, or nutrient deprivation [36, 37, 35]. Despite these insights, the interplay between NGB and cholesterol metabolism remains largely unexplored, representing a critical gap given the influence of cholesterol on membrane dynamics, lipid signaling, and stress responses in brain cells. This study revealed that NGB overexpression seems to remodel cholesterol homeostasis in neuronal-like SH-SY5Y cells and, to a greater extent, in astrocyte-like U373 cells. In SH-SY5Y cells, NGB increases total and nuclear SREBP2, HMGCR protein, cholesterol uptake markers, and lysosomal cholesterol accumulation while simultaneously reducing SREBP1 activity, SQS, ACC, and neutral lipid content. In U373 cells, NGB also increases cholesterol accumulation but with a distinct pattern of metabolic regulation, highlighting that the effects of NGB on lipid homeostasis are strongly cell dependent. Overall, these data indicate that NGB does not simply increase or decrease cholesterol levels but rather may reshape the intracellular routes by which cholesterol is synthesized, imported, and compartmentalized.

Mechanistically, although the approach, which is based on filipin staining and total cholesterol quantification, primarily reflects steady-state levels and does not allow us to discriminate between synthesis, uptake, and efflux, it has been hypothesized that, in SH-SY5Y cells, NGB may shift cholesterol metabolism away from *de novo* lipogenesis and toward receptor-mediated uptake and lysosomal trapping. Although SREBP2 and HMGCR are increased, HMGCR activity appears to be functionally restrained by AMPK-dependent phosphorylation, which is consistent with a partial uncoupling between enzyme abundance and enzymatic activity [23]. Moreover, SREBP1 suppression is accompanied by reduced SQS and ACC, supporting a broader inhibition of lipogenic programs and neutral lipid synthesis [24]. This is important because it could help explain why lipid droplets do not expand despite increased cholesterol availability [38]. Instead, cholesterol appears to accumulate in the endolysosomal system, where increased LDLR, LRP1, APOE, and TMEM97, together with reduced SR-B1 and APOA1, could favor the internalization and intracellular retention of lipoprotein-derived cholesterol rather than HDL-like lipid exchange or efflux [4, 30, 37]. This interpretation is consistent with the neuronal context, where cholesterol homeostasis is tightly dependent on glial-derived lipoproteins and receptor-mediated trafficking [2]. In neurons, APOE is the major cholesterol carrier in the CNS, and SR-B1 supports selective lipid transfer with relatively limited holoparticle uptake [39]. In contrast, increased LDLR, LRP1, APOE, and TMEM97 may promote a more endocytic, bulk-internalization phenotype that delivers cholesterol into the cell but increases the risk of lysosomal entrapment when downstream egress is compromised [40]. In this context, the decrease in NPC1 and the expansion of LAMP2-positive compartments provide a plausible explanation for the accumulation of cholesterol in lysosomes. The ability of β-cyclodextrin to reverse SREBP2 alteration further suggests that cholesterol is trapped in the lysosomal compartment rather than being freely distributed in the cytosol or incorporated into neutral lipid droplets [41].

The relationship between NGB and AMPK is more difficult to interpret and should be treated with caution. One possibility is that NGB affects cellular energy sensing indirectly, leading to AMPK

activation despite the overall increase in ATP content previously demonstrated [44]. This is not necessarily contradictory because AMPK can be activated by mechanisms other than global AMP/ATP changes, including CaMKK2-dependent signaling, redox changes, and local metabolic fluctuations [42]. In neurons, compartmentalized energy demands may allow regional AMPK activation even when total cellular ATP is elevated [43]. Therefore, the observed increase in AMPK activity may reflect adaptive metabolic remodeling rather than a classical energy crisis. This adaptive signaling could contribute to reduced SREBP1 activity [44, 43] and altered NPC1 expression [25], as well as the observed shift toward lysosomal cholesterol retention. Therefore, the role of AMPK in this model needs to be further investigated.

These findings in U373 cells support the idea that NGB acts in a cell type-specific manner. In astrocytes, NGB increases HMGCR, SQS, APOE, and NPC1 without a detectable change in SREBP2, yet cholesterol still accumulates. These findings suggest that astrocytes and neurons may differ in how they integrate NGB-dependent signals at the level of transcriptional control, cholesterol trafficking, and compartmental storage. Importantly, conditioned media from astrocyte-like cells improved neuronal survival, in agreement with the well-established role of astrocytes in supporting neuronal health. This effect is consistent with previous evidence [31], indicating that astrocyte-derived factors, including ApoE-containing lipoproteins, contribute to neuronal metabolic support and structural integrity, although this aspect was not directly investigated in the present work. In this context, compared with control cells, NGB-overexpressing U373-overexpressing cells exhibited no additional improvement when the neurons were exposed to conditioned media. These findings suggest that under our experimental conditions, NGB overexpression does not further enhance the intrinsic neurosupportive properties of astrocytes. Although the possibility that NGB may modulate specific aspects of astrocyte-neuron communication cannot be excluded, the data indicate that such effects do not translate into measurable changes in neuronal survival or morphology. Further studies will be needed to determine whether more subtle mechanisms, including the modulation of lipid trafficking or ApoE-dependent signaling, may be involved. These

data are broadly consistent with studies showing that lysosomal cholesterol enrichment can be protective under stress. Cholesterol-rich lysosomes may better withstand oxidative or mitochondrial insults by increasing membrane rigidity, limiting membrane damage, and buffering lipid peroxidation [45, 46]. Similar protective effects have been described in models involving NPC1 dysfunction or pharmacological cholesterol trapping, where transient lysosomal cholesterol accumulation can preserve cell viability under stress [47, 48]. From this perspective, NGB-induced lysosomal cholesterol retention may represent an adaptive response that contributes to the neuroprotective effect of NGB [14, 18]. However, this view must be balanced against the well-established toxicity of chronic cholesterol overload. Persistent lysosomal cholesterol accumulation can reproduce features of Niemann–Pick C pathology, impair cholesterol esterification, and promote secondary defects in autophagy, lipofuscin accumulation, and protein aggregation [41, 49]. These results therefore support a model in which NGB promotes a short-term protective lipid-buffering state, but the long-term consequences of sustained cholesterol retention remain uncertain (Fig. 8). This distinction is important because the same mechanism that stabilizes lysosomes during acute stress could become maladaptive if it is maintained chronically. In that case, increased APOE-cholesterol handling, defective NPC1-dependent export, and persistent lysosomal expansion might eventually contribute to proteostasis defects or to broader neurodegenerative vulnerability. The present data do not allow us to determine whether NGB shifts cells toward a protective transient state or toward a chronically maladaptive state, and this will require time-resolved experiments. Nonetheless, considering the inducible nature of the NGB protein, it can be hypothesized that, beyond conditions of overexpression, under physiological conditions, the acute and regulated increase in NGB expression occurring in response to stress [13, 14, 16] or upon cell exposure to NGB inducers (e.g., hormones) [13, 18] may activate the cytoprotective function of globin, which, as indicated by the present data, may also rely on a transient enrichment of cholesterol. In broader terms, these findings suggest that NGB may influence neuronal resilience not only through classical antioxidant or anti-apoptotic pathways [18] but also by reshaping lipid metabolism and lysosomal

cholesterol handling. These findings add a metabolic dimension to NGB biology and raise the possibility that part of its neuroprotective activity is linked to the controlled modulation of membrane lipid composition and organelle stability. Notably, diseases associated with cholesterol metabolism, such as Alzheimer's disease, atherosclerosis, and ischemia, are mitigated by the upregulation of NGB [15, 17].

5. Limitations of the study

Several limitations should be considered. First, the *in vitro* cell models used in this study cannot fully reproduce the complexity of the CNS, including multicellular interactions, tissue architecture, and systemic lipid metabolism. Second, the use of an overexpression system may introduce nonphysiological effects, especially given the high increase in NGB achieved in our model. Third, the study lacks direct flux measurements; thus, whether the changes observed reflect altered synthesis, uptake, redistribution, storage, or degradation of cholesterol is unclear. In particular, measurements of lipid flux, receptor turnover, and compartment-specific cholesterol movement are necessary to confirm the proposed trafficking model. Fourth, astrocyte–neuron cross-talk was assessed only through conditioned media, which captures soluble factors but not direct contact-dependent or vesicle-mediated interactions.

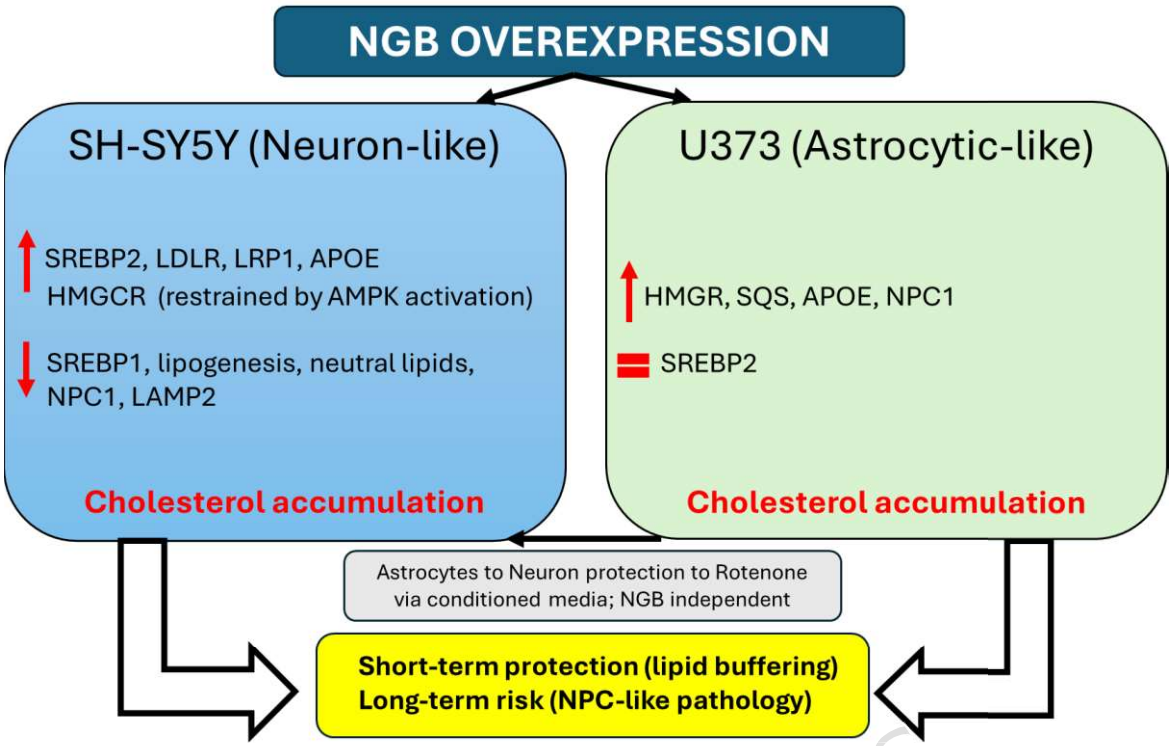

Figure 8. Schematic diagram of the effects of NGB on cholesterol metabolism in SH-SY5Y and U373 cells.

6. Conclusions

If our model is validated in more physiological systems, NGB-based strategies could be used to induce a transient lipid-buffering state that protects neurons under stress without triggering chronic lipid toxicity. Moreover, the present results caution that sustained cholesterol trapping could have adverse consequences; thus, therapeutic approaches need to carefully balance protection against long-term metabolic risk.

Declarations

Ethics approval and consent to participate: The study was exempt from ethical approval since it was performed on *in vitro* cell lines.

Consent for publication: Not applicable (no individual patient data/images included).

Availability of data and materials: All the data generated are available from the corresponding author upon request.

Competing interests: The authors declare that they have no competing interests.

Funding: This work was funded by Missione 6/Componente 2/Investimento 2.1 'Rafforzamento e potenziamento della ricerca biomedica del SSN' EU – Next generation EU CUP J83C220020300007.

Authors' contributions: Conceptualization: VP, MS; Data curation: SC, MP, MS, MC, MF, MM, VP; Formal Analysis: SC,MP, VP, MS, MC; Funding acquisition: MM; Investigation: SC,MP,MC, Methodology: SC, MP, MC,MS, ; Project administration MM Resources: MM, MS, VP; Supervision: VP; MS Writing – original draft: VP; Writing – review & editing: SC, MP, MC, MS, MF, MM, VP. All authors have read and agreed to the published version of the manuscript.

Acknowledgments: We thank Dr. F.W. Pfrieger, Group Leader,Institute of Cellular and Integrative Neurosciences (INCI), CNRS UPR 3212, Universite de Strasbourg for the fruitful discussions.

References

1 C. Martini and V. Pallottini, “Cholesterol: from feeding to gene regulation,” *Genes Nutr*, vol. 2, no. 2, pp. 181–193, Oct. 2007, doi: 10.1007/s12263-007-0049-y.

2 F. W. Pfrieger and N. Ungerer, “Cholesterol metabolism in neurons and astrocytes,” *Prog Lipid Res*, vol. 50, no. 4, pp. 357–371, Oct. 2011, doi: 10.1016/j.plipres.2011.06.002.

3 M. G. Martín, F. Pfrieger, and C. G. Dotti, “Cholesterol in brain disease: sometimes determinant and frequently implicated,” *EMBO Rep*, vol. 15, no. 10, pp. 1036–1052, Oct. 2014, doi: 10.15252/embr.201439225.

4 M. Parente, C. Tonini, S. Caputo, M. Fiocchetti, and V. Pallottini, “Mechanisms of Sigma-2/TMEM97 Involvement in Cholesterol Metabolism,” *J Cell Biochem*, vol. 125, no. 10, p. e30645, Oct. 2024, doi: 10.1002/jcb.30645.

5 S. Member and M. Bruger, “Experimental atherosclerosis; the effect of feeding olive oil on the absorption and deposition of cholesterol,” *Arch Pathol (Chic)*, vol. 40, pp. 373–375, 1945.

6 G. Luden, “The Blood Cholesterol-Its Importance, and the Value of its Determination in Cancer Research,” *Can Med Assoc J*, vol. 12, no. 3, pp. 147–152, Mar. 1922.

7 J. Guo *et al.*, “Cholesterol metabolism: physiological regulation and diseases,” *MedComm*, vol. 5, no. 2, p. e476, Feb. 2024, doi: 10.1002/mco2.476.

8 W. Y. Ho, H. Hartmann, and S.-C. Ling, “Central nervous system cholesterol metabolism in health and disease,” *IUBMB Life*, vol. 74, no. 8, pp. 826–841, Aug. 2022, doi: 10.1002/iub.2662.

9 M. Segatto, L. Leboffe, L. Trapani, and V. Pallottini, “Cholesterol Homeostasis Failure in the Brain: Implications for Synaptic Dysfunction and Cognitive Decline,” *CMC*, vol. 21, no. 24, pp. 2788–2802, Jul. 2014, doi: 10.2174/09298673216661403031429 02.

10 M. Menendez-Gonzalez, “Therapeutic Challenges Derived from the Interaction Among Apolipoprotein E, Cholesterol, and Amyloid in Alzheimer’s Disease,” *IJMS*, vol. 25, no. 22, p. 12029, Nov. 2024, doi: 10.3390/ijms252212029.

11 M. Valenza and E. Cattaneo, “Emerging roles for cholesterol in Huntington’s disease,” *Trends in Neurosciences*, vol. 34, no. 9, pp. 474–486, Sep. 2011, doi: 10.1016/j.tins.2011.06.005.

12 K. C. Shin, H. Y. Ali Moussa, and Y. Park, “Cholesterol imbalance and neurotransmission defects in neurodegeneration,” *Exp Mol Med*, vol. 56, no. 8, pp. 1685–1690, Aug. 2024, doi: 10.1038/s12276-024-01273-4.

13 P. Ascenzi *et al.*, “Neuroglobin: From structure to function in health and disease,” *Molecular Aspects of Medicine*, vol. 52, pp. 1–48, Dec. 2016, doi: 10.1016/j.mam.2016.10.004.

14 G. Bastari, V. Solar Fernandez, M. Muzzi, S. Moreno, M. Marino, and M. Fiocchetti, “Neuroglobin-enriched secretome provides neuroprotection against hydrogen peroxide and mitochondrial toxin-induced cellular stress,” *Cell Stress*, vol. 8, pp. 99–111, 2024, doi: 10.15698/cst2024.11.300.

15 Z. P. Van Acker *et al.*, “Impaired hypoxic tolerance in APP 23 mice: a dysregulation of neuroprotective globin levels,” *FEBS Letters*, vol. 591, no. 10, pp. 1321–1332, May 2017, doi: 10.1002/1873-3468.12651.

16 I. M. Yañez, I. Torres-Cuevas, and M. Corral-Debrinski, “Neuroglobin: A promising candidate to treat neurological diseases,” *Neural Regeneration Research*, Jun. 2025, doi: 10.4103/NRR.NRR-D-24-01503.

17 E. Luyckx *et al.*, “Cytoprotective effects of transgenic neuroglobin overexpression in an acute and chronic mouse model of ischemic heart disease,” *Heart Vessels*, vol. 33, no. 1, pp. 80–88, Jan. 2018, doi: 10.1007/s00380-017-1065-5.

18 P. Cracco *et al.*, “A Novel Resveratrol-Induced Pathway Increases Neuron-Derived Cell Resilience against Oxidative Stress,” *IJMS*, vol. 24, no. 6, p. 5903, Mar. 2023, doi: 10.3390/ijms24065903.

19 M. Costanzo, M. Fiocchetti, P. Ascenzi, M. Marino, M. Caterino, and M. Ruoppolo, "Proteomic and Bioinformatic Investigation of Altered Pathways in Neuroglobin-Deficient Breast Cancer Cells," *Molecules*, vol. 26, no. 8, p. 2397, Apr. 2021, doi: 10.3390/molecules26082397.

20 F. M. Harris *et al.*, "Astroglial regulation of apolipoprotein E expression in neuronal cells. Implications for Alzheimer's disease," *J Biol Chem*, vol. 279, no. 5, pp. 3862–3868, Jan. 2004, doi: 10.1074/jbc.M309475200.

21 M. Parente *et al.*, "Exploration of Bromodomain Proteins as Drug Targets for Niemann-Pick Type C Disease," *Int J Mol Sci*, vol. 26, no. 12, p. 5769, Jun. 2025, doi: 10.3390/ijms26125769.

22 J. L. Goldstein and M. S. Brown, "Molecular medicine. The cholesterol quartet," *Science*, vol. 292, no. 5520, pp. 1310–1312, May 2001, doi: 10.1126/science.1061815.

23 D. G. Hardie, "Minireview: the AMP-activated protein kinase cascade: the key sensor of cellular energy status," *Endocrinology*, vol. 144, no. 12, pp. 5179–5183, Dec. 2003, doi: 10.1210/en.2003-0982.

24 G. Guan, P. Dai, and I. Shechter, "Differential Transcriptional Regulation of the Human Squalene Synthase Gene by Sterol Regulatory Element-binding Proteins (SREBP) 1a and 2 and Involvement of 5′ DNA Sequence Elements in the Regulation," *Journal of Biological Chemistry*, vol. 273, no. 20, pp. 12526–12535, May 1998, doi: 10.1074/jbc.273.20.12526.

25 M. Segatto *et al.*, "Cholesterol Metabolism Is Altered in Rett Syndrome: A Study on Plasma and Primary Cultured Fibroblasts Derived from Patients," *PLoS ONE*, vol. 9, no. 8, p. e104834, Aug. 2014, doi: 10.1371/journal.pone.0104834.

26 P. J. Espenshade and A. L. Hughes, "Regulation of sterol synthesis in eukaryotes," *Annu Rev Genet*, vol. 41, pp. 401–427, 2007, doi: 10.1146/annurev.genet.41.110306.130315.

27 F. W. Pfrieger, “The Niemann-Pick type diseases - A synopsis of inborn errors in sphingolipid and cholesterol metabolism,” *Prog Lipid Res*, vol. 90, p. 101225, Apr. 2023, doi: 10.1016/j.plipres.2023.101225.

28 N. Gévry, K. Schoonjans, F. Guay, and B. D. Murphy, “Cholesterol supply and SREBPs modulate transcription of the Niemann-Pick C-1 gene in steroidogenic tissues,” *J Lipid Res*, vol. 49, no. 5, pp. 1024–1033, May 2008, doi: 10.1194/jlr.M700554-JLR200.

29 D. Ebrahimi-Fakhari *et al.*, “Reduction of TMEM97 increases NPC1 protein levels and restores cholesterol trafficking in Niemann-pick type C1 disease cells,” *Hum. Mol. Genet.*, vol. 25, no. 16, pp. 3588–3599, Aug. 2016, doi: 10.1093/hmg/ddw204.

30 A. Riad *et al.*, “Sigma-2 Receptor/TMEM97 and PGRMC-1 Increase the Rate of Internalization of LDL by LDL Receptor through the Formation of a Ternary Complex,” *Sci Rep*, vol. 8, no. 1, p. 16845, Nov. 2018, doi: 10.1038/s41598-018-35430-3.

31 M. Colardo *et al.*, “NGF Modulates Cholesterol Metabolism and Stimulates ApoE Secretion in Glial Cells Conferring Neuroprotection against Oxidative Stress,” *Int J Mol Sci*, vol. 23, no. 9, p. 4842, Apr. 2022, doi: 10.3390/ijms23094842.

32 B. M. Kelser, E. M. Teichner, R. C. Subtirelu, and K. N. Hoss, “A review of proposed mechanisms for neurodegenerative disease,” *Front Aging Neurosci*, vol. 16, p. 1370580, 2024, doi: 10.3389/fnagi.2024.1370580.

33 L. Zhang, D. Li, L. Yin, C. Zhang, H. Qu, and J. Xu, “Neuroglobin protects against cerebral ischemia/reperfusion injury in rats by suppressing mitochondrial dysfunction and endoplasmic reticulum stress-mediated neuronal apoptosis through synaptotagmin-1,” *Environmental Toxicology*, vol. 38, no. 8, pp. 1891–1904, Aug. 2023, doi: 10.1002/tox.23815.

34 H. Cwerman-Thibault *et al.*, “Neuroglobin overexpression in cerebellar neurons of Harlequin mice improves mitochondrial homeostasis and reduces ataxic behavior,” *Molecular Therapy*, vol. 32, no. 7, pp. 2150–2175, Jul. 2024, doi: 10.1016/j.ymthe.2024.05.030.

35 M. Á. Peinado *et al.*, "Does Neuroglobin Protect Against Stroke? Insights Into the Role of Neurovascular Unit Cells," *Cell Mol Neurobiol*, vol. 46, no. 1, p. 23, Jan. 2026, doi: 10.1007/s10571-025-01656-9.

36 Y. Li *et al.*, "Neuroglobin Attenuates Beta Amyloid-Induced Apoptosis Through Inhibiting Caspases Activity by Activating PI3K/Akt Signaling Pathway," *J Mol Neurosci*, vol. 58, no. 1, pp. 28–38, Jan. 2016, doi: 10.1007/s12031-015-0645-z.

37 A. A. Khan, X. O. Mao, S. Banwait, K. Jin, and D. A. Greenberg, "Neuroglobin attenuates beta-amyloid neurotoxicity *in vitro* and transgenic Alzheimer phenotype *in vivo*," *Proc Natl Acad Sci U S A*, vol. 104, no. 48, pp. 19114–19119, Nov. 2007, doi: 10.1073/pnas.0706167104.

38 J. D. Horton, "Sterol regulatory element-binding proteins: transcriptional activators of lipid synthesis," *Biochem Soc Trans*, vol. 30, no. Pt 6, pp. 1091–1095, Nov. 2002, doi: 10.1042/bst0301091.

39 S. Riedel *et al.*, "Exercise training improves high-density lipoprotein-mediated transcription of proangiogenic microRNA in endothelial cells," *Eur J Prev Cardiol*, vol. 22, no. 7, pp. 899–903, Jul. 2015, doi: 10.1177/2047487314541036.

40 D. Vance, "Cholesterol in the year 2000," *Biochimica et Biophysica Acta (BBA) - Molecular and Cell Biology of Lipids*, vol. 1529, no. 1–3, pp. 1–8, Dec. 2000, doi: 10.1016/S1388-1981(00)00133-5.

41 J. E. Vance and B. Karten, "Niemann-Pick C disease and mobilization of lysosomal cholesterol by cyclodextrin," *J Lipid Res*, vol. 55, no. 8, pp. 1609–1621, Aug. 2014, doi: 10.1194/jlr.R047837.

42 V. Manganelli *et al.*, "Neuroglobin regulates autophagy through mTORC1/RAPTOR/ULK-1 pathway in human neuroblastoma cells," *Sci Rep*, vol. 15, no. 1, p. 7642, Mar. 2025, doi: 10.1038/s41598-025-91701-w.

43 T. Feofilaktova, L. Kushnireva, M. Segal, and E. Korkotian, “Calcium signaling in postsynaptic mitochondria: mechanisms, dynamics, and role in ATP production,” *Front Mol Neurosci*, vol. 18, p. 1621070, 2025, doi: 10.3389/fnmol.2025.1621070.

44 B. Chen *et al.*, “Suppression of hepatosteatosis by isarubrolone C through AMPK-dependent regulation of lipophagy and lipid metabolism,” *Metabolism*, vol. 176, p. 156487, Mar. 2026, doi: 10.1016/j.metabol.2025.156487.

45 T. Kolter and K. Sandhoff, “Principles of lysosomal membrane digestion: stimulation of sphingolipid degradation by sphingolipid activator proteins and anionic lysosomal lipids,” *Annu Rev Cell Dev Biol*, vol. 21, pp. 81–103, 2005, doi: 10.1146/annurev.cellbio.21.122303.120013.

46 E. Lloyd-Evans *et al.*, “Niemann-Pick disease type C1 is a sphingosine storage disease that causes deregulation of lysosomal calcium,” *Nat Med*, vol. 14, no. 11, pp. 1247–1255, Nov. 2008, doi: 10.1038/nm.1876.

47 H. Appelqvist *et al.*, “Sensitivity to lysosome-dependent cell death is directly regulated by lysosomal cholesterol content,” *PLoS One*, vol. 7, no. 11, p. e50262, 2012, doi: 10.1371/journal.pone.0050262.

48 I. Caria *et al.*, “NPC1-like phenotype, with intracellular cholesterol accumulation and altered mTORC1 signaling in models of Parkinson’s disease,” *Biochimica et Biophysica Acta (BBA) - Molecular Basis of Disease*, vol. 1870, no. 2, p. 166980, Feb. 2024, doi: 10.1016/j.bbadis.2023.166980.

49 V. Pallottini and F. W. Pfrieger, “Understanding and Treating Niemann–Pick Type C Disease: Models Matter,” *IJMS*, vol. 21, no. 23, p. 8979, Nov. 2020, doi: 10.3390/ijms21238979.